HHS Public Access

Author manuscript

Nat Chem Biol. Author manuscript; available in PMC 2019 March 17.

Published in final edited form as:

Nat Chem Biol. 2018 October ; 14(10): 934–942. doi:10.1038/s41589-018-0130-4.

T cell receptor cross-reactivity expanded by dramatic peptide/MHC adaptability

Timothy P. Riley[1,2], **Lance M. Hellman**[1,2], **Marvin H. Gee**[3,4], **Juan L. Mendoza**[3,4], **Jesus A. Alonso**[3,4], **Kendra C. Foley**[5], **Michael. I. Nishimura**[5], **Craig W. Vander Kooi**[6], **K. Christopher Garcia**[3,4], and **Brian M. Baker**[1,2,*]

[1]Department of Chemistry and Biochemistry, University of Notre Dame, Notre Dame, IN, USA

[2]Harper Cancer Research Institute, University of Notre Dame, Notre Dame, IN, USA

[3]Department of Molecular and Cellular Physiology, Stanford University School of Medicine, Stanford, CA, USA

[4]Department of Structural Biology, Stanford University School of Medicine, Stanford, CA, USA

[5]Department of Surgery, Cardinal Bernardin Cancer Center, Loyola University Chicago, Maywood, IL, USA

[6]Department of Molecular and Cellular Biochemistry, University of Kentucky, Lexington, KY, USA

Abstract

T cell receptor cross-reactivity allows a fixed T cell repertoire to respond to a much larger universe of potential antigens. Recent work has emphasized the importance of peptide structural and chemical homology, as opposed to sequence similarity, in T cell receptor cross-reactivity. Surprisingly though, T cell receptors can also cross-react between ligands with little physiochemical commonalities. Studying the clinically relevant receptor DMF5, we demonstrate that cross-recognition of such divergent antigens can occur through mechanisms that involve heretofore unanticipated rearrangements in the peptide and presenting MHC protein, including binding-induced peptide register shifts and extensions from MHC peptide binding grooves. Moreover, cross-reactivity can proceed even when such dramatic rearrangements do not translate into structural or chemical molecular mimicry. Beyond demonstrating new principles of T cell receptor cross-reactivity, our results have implications for efforts to predict and control T cell specificity and cross-reactivity, and highlight challenges associated with predicting T cell reactivities.

*Corresponding author: brian-baker@nd.edu.

Author contributions

Modeling, crystallographic, and TCR binding experiments were performed by T.P.R., L.M.H., and J.A.A. C.W.V.K assisted with crystallographic data collection and analysis. Thermal stability experiments were performed by T.P.R. and L.M.H. Functional experiments were performed by L.M.H. with assistance from K.C.F. in T cell transduction. Data analysis was performed by T.P.R., L.M.H., M.H.G., J.L.M., J.A.A., and C.W.V.K. The manuscript was drafted and edited by T.P.R., M.H.G., J.L.M., and B.M.B. The project was conceptualized by T.P.R., K.C.G., and B.M.B. Personnel were supervised by M.I.N., K.C.G., and B.M.B.

Competing financial interests

T.P.R. is employed by a new startup company that uses structural information to explore and modulate TCR specificity. B.M.B. is on the board of this company.

Introduction

αβ T cell receptors (TCRs) recognize short peptides bound and presented by major histocompatibility complex (MHC) proteins. While specificity is a hallmark of the immune system, TCRs themselves recognize multiple peptide/MHC complexes. TCR cross-reactivity, or polyspecificity [1], is a necessity arising from the fixed size of an individual's TCR repertoire relative to the much larger universe of potential antigens. Early predictions of the scope of cross-reactivity suggested TCRs need to recognize on average at least 1 million peptides to confer immunity [2, 3], a value supported by experimental and structural analyses [4–6]. Beyond its role in the normal function of the immune system, cross-reactivity hinders the development of TCRs as therapeutics due to its potential to introduce off-target immune toxicity [7].

Although a target size in the millions comprises a considerable number of ligands, the composition of TCR target pools will not be random but governed by the structural and physicochemical properties of each TCR. As with other protein-protein interfaces, TCR-pMHC interfaces contain "hot spots" that limit chemical and structural diversity. For example, libraries of ligands for the 2B4 and 42F3 TCRs revealed constraints on the residues at a subset of peptide positions, and structural analyses indicated the residues at these positions participated in similar contact networks with the TCR binding loops [8, 9]. Similar results were found with the 1E6 TCR [10]. Such constraints were demonstrated in even earlier work: the binding of the archetypal anti-viral TCR A6 was shown to depend critically on the identity of peptide residues 4 and 8, with substantial variation tolerated elsewhere [11–14].

Integrating the concepts of hot spots with other peptide constraints permits rationalizations and predictions about the makeup of ligands for a given TCR [5]. However, these rationalizations and predictions are predicated on the notion that the pool of ligands for a given TCR is built around core regions of restricted structural and chemical space [5, 6, 15]. Yet is it possible that TCRs could productively engage multiple ligand pools, each defined by distinct structural/chemical cores? Hints of this behavior, which most closely captures the concept of polyspecificity, have been detected in studies with peptide libraries [16, 17], and it has been suggested to be particularly important in heterologous immunity and memory [18, 19]. Protein adaptability, which is often observed in studies of TCR recognition [20, 21], could be one mechanism that contributes to recognition of diverse ligands.

The DMF5 TCR recognizes the MART-1 melanoma antigen presented by the class I MHC protein HLA-A*0201 [22]. DMF5 is a well-characterized TCR and has been used in clinical trials of gene-modified T cells [23, 24]. Structural and biophysical studies of DMF5 revealed a relatively rigid molecule [25, 26], hypothetically limiting the capacity of the receptor to engage very different peptides. Yet specificity profiling through yeast-display of peptide-MHC libraries revealed that the TCR recognized two distinct classes of peptides [27]. One class was characteristic of MART-1, typified by a hydrophobic motif in the peptide core. The second class of peptides, however, differed substantially from the MART-1-type peptides, possessing a central core dominated by charged amino acids.

Here we asked how a TCR such as DMF5 can productively engage two very different classes of antigens. Unexpectedly, we found that cross-recognition is governed by a binding-induced “register shift” in the charged peptide class that leads to a peptide C-terminal extension from the class I MHC binding groove. The features of the register shifted peptide remain structurally and chemically distinct from the MART-1 epitope, indicating true TCR accommodation of a new surface as opposed to molecular mimicry induced by conformational change. These results have significant implications for ongoing efforts to account for, predict, and control TCR specificity and cross-reactivity in fields ranging from autoimmunity, alloreactivity, and immunotherapy, and highlight the potentially dangerous limitations of relying on sequence or other limited data to predict and assess T cell reactivities.

Results

Two distinct classes of DMF5-reactive peptides

Specificity profiling of the DMF5 TCR through yeast display of peptide-MHC libraries revealed dozens of distinct peptides after four rounds of selection [27]. Although not an exhaustive screen, these peptides separated into two divergent classes which we term GIG or DRG, reflecting the strongly conserved sequences found at positions 4-6 of the two peptide classes (Figure 1A). A dendrogram of the top 9 peptides, accounting for 95% of those identified, along with the MART-1 anchor modified decamer (ELAGIGILTV), highlights the distinctive nature of the two classes (Figure 1B). While it is unknown whether peptides in the DRG-class represent physiological targets, peptides matching the DRG-motif are present in numerous genomes (Supplementary Table 1).

To assess the structural features of the peptides in the HLA-A2 binding groove, we computationally modeled and scored the GIG and DRG peptides in the HLA-A2 peptide binding groove [28, 29]. The models of the GIG class all closely resembled the previously crystallized decameric MART-1/HLA-A2 complex [30, 31]. The structures of the DRG peptides, on the other hand, were predicted to differ substantially, with a larger bulge across the peptide center, leading to an average GIG/DRG backbone root mean square deviation (RMSD) of 1.8 Å (Figure 1C). Consistent with a structural divergence, the affinities of the GIG and DRG peptides for HLA-A2 diverged when measured using differential scanning fluorimetry: on average, the T_m values of the DRG peptide/HLA-A2 complexes were 12 °C lower than those of the GIG complexes, indicating weaker peptide binding (Figure 1D; Supplementary Table 2). The T_m values correlated well with the energetic scores of the peptide/MHC models, supporting the conclusion that weaker binding of the DRG peptides to HLA-A2 is attributable to divergent structural features.

The MMWDRGLGMM/HLA-A2 complex is structurally distinct

To further investigate the differences between the GIG and DRG peptides, we determined the crystallographic structure of the peptide most distinct from the MART-1 decamer, MMWDRGLGMM, bound to HLA-A2 (Supplementary Table 4; Supplementary Figure 1A). The MMWDRGLGMM/HLA-A2 complex crystallized with two molecules in the asymmetric unit. The refined positions of the two copies were essentially identical, with the

peptide backbones superimposing with a RMSD of 0.6 Å. The electron density clearly showed that the second and last methionines were utilized as the first and last primary anchors, respectively.

As suggested by the structural models, the conformation of MMWDRGLGMM bound to HLA-A2 binding groove differed substantially from the MART-1 decamer (Figure 2A). The p3 tryptophan (alanine in MART-1) pushes the peptide backbone towards the α1 helix. The peptide C-terminal half is more bulged, due in part to the suboptimal methionine at p10 (valine in MART-1) that elevates the peptide backbone away from the binding groove floor. Additionally, unlike the p7 isoleucine in MART-1, the p7 leucine in MMWDRGLGMM is oriented towards the base of the groove, close to the usual position of Val152. This induces a displacement in the short arm of the HLA-A2 α2 helix, beginning near Val152 and continuing through His145 (Figure 2B). The displacement is maximal at Ala150, widening the binding groove by 2 Å at this point. Overall, the MMWDRGLGMM/HLA-A2 structure confirms that the peptides in the DRG and GIG classes are not molecular mimics, differing not only in sequence, but also in conformation and their impacts on HLA-A2 structure (Figure 2C).

DMF5 binds the peptide classes via distinct mechanisms

We next used biophysical and functional assays to ask if the differences between the GIG and DRG peptides impact TCR recognition. We measured TCR binding affinities using surface plasmon resonance (SPR), utilizing a global analysis approach optimized for moderate-to-weak binding affinities as described in the Methods. These experiments showed that, unlike pMHC stabilities, TCR binding affinities did not cleanly segregate by peptide class: K_D values ranged from 5 μM to 200 μM, and peptides in both the GIG and DRG classes were found at both ends of the range (Figure 3A; Supplementary Table 2). The binding measurements were mirrored in functional assays, where the extent of IFNγ release by DMF5-transduced T cells incubated with peptide-pulsed targets correlated well with TCR affinity (Figure 3B).

Although the DMF5 TCR did not display a preference for either peptide class, kinetic measurements suggested distinct mechanisms of binding. As reported previously for the binding of DMF5 to the MART-1 decamer [25], TCR association and dissociation rates for GIG peptides were rapid and not quantifiable. The on- and off-rates for TCR binding to the DRG peptides, on the other hand, were slower and could be accurately measured (Figure 3C; see also Supplementary Figure 2).

Noting the perturbation in the HLA-A2 α2 helix observed in the MMWDRGLGMM/HLA-A2 crystal structure, we next investigated the role that the MHC α2 helix conformation plays in DMF5 recognition. Previously, we mutated alanine 150 in the α2 helix to proline in order to “lock” the short arm of the HLA-A2 α2 helix into an alternate configuration, validating the role of HLA-A2 conformational changes in binding of the A6 TCR to different ligands [14]. Here, the A150P mutation only slightly impacted binding of DMF5 to MART-1/HLA-A2 ($\Delta\Delta G^\circ$ = 0.4 kcal/mol), but dramatically inhibited recognition of MMWDRGLGMM ($\Delta\Delta G^\circ$ > 2 kcal/mol) (Figure 3D). This differential result of the A150P

mutation confirms that peptide-dependent adjustments in HLA-A2 facilitate DMF5 recognition of the different peptide classes.

DMF5 binds GIG class peptides with a common solution

To more critically examine how DMF5 can engage the two classes of peptides, we determined the structures of DMF5 in complex with select GIG and DRG peptides. The complex with the representative GIG peptide, SMLGIGIVPV, was solved at 2.4 Å (Supplementary Table 4; Supplementary Figure 1B). The SMLGIGIVPV peptide conformation is nearly identical to that of the MART-1 peptide in the ternary complex with DMF5 and HLA-A2 (backbone RMSD of 0.5 Å when the HLA-A2 peptide binding domains were superimposed) [25]. Indeed, the DMF5-SMLGIGIVPV/HLA-A2 complex is virtually the same as the DMF5-MART-1/HLA-A2 complex, with no significant perturbations in side chains, CDR loops, or TCR docking (Figure 4). The SMLGIGIVPV peptide forms many of the same interactions with DMF5 as does MART-1, including hydrogen bonds from peptide positions 2 and 3 to Gln30 in CDR1α, and the complexes both incorporate the same key water molecule that bridges the TCR and peptide center [25]. Thus, the DMF5 TCR engages the GIG peptides with a common structural solution, reflecting how the shared peptide conformation and the central GIG core facilitate cross-recognition.

Dramatic changes on binding the DRG peptide

We next determined the structure of DMF5 bound to the DRG-class peptide MMWDRGLGMM (Supplementary Table 4). This complex displayed remarkably different properties compared to the MART-1 and SMLGIGIVPV complexes. The electron density indicated that the MMWDRGLGMM C-terminus was “register shifted” compared to its configuration in the free pMHC, with the methionine at p9 (as opposed to the methionine at p10) occupying the HLA-A2 F pocket (Figure 5A; Supplementary Figure 1C). The register shift leads to a less bulged conformation more typically seen with nonameric peptides bound to class I MHC proteins. From a structural perspective, the TCR forces a 7 Å movement in the p5 arginine side chain to a position overlapping with pGly6. To avoid clashing, the backbone at p6-p8 shifts down towards the base of the groove by 5 Å, popping the pMet10 side chain up and out of the groove and allowing pMet9 to occupy the F pocket. The large change in peptide conformation is reflected in the RMSD of 3.5 Å for all peptide atoms when the bound and free HLA-A2 peptide binding domains are superimposed.

The peptide shift brings the backbone conformation closer to, but not coincident with the conformation of the GIG peptides when bound to DMF5 (Figure 5B, upper panel). Indeed, comparing the peptide surfaces in the TCR-bound states indicates that cross-reactivity between the GIG and DRG peptides is not “induced-fit molecular mimicry” [32], as the TCR-exposed surfaces remain distinct (Figure 5B, lower panel), with different TCR-peptide contacts (Supplementary Figure 3). An animation of the TCR-induced register shift in the peptide is available as Supplementary Video 1.

In the MMWDRGLGMM ternary complex the HLA-A2 α2 helix returns to its more traditional configuration, associated with a shift of the p7 leucine back towards the groove center (Figure 5C). The Lys146 side chain, which has been previously described as a “lid”

over the peptide C-terminus in class I MHC proteins [33], is also shifted closer to the peptide C-terminus. As these HLA-A2 conformational shifts occur together with the peptide register shift, we hypothesize that the less-stable conformation MMWDRGLGMM induces in unbound HLA-A2 (Figure 2B) is more dynamic and relaxed, which helps facilitate the conformational changes that occur upon TCR binding.

To validate the peptide register shift, we examined variants of the MMWDRGLGMM peptide. The first was a variant in which the p9 methionine was replaced with alanine. As alanine is a suboptimal anchor for HLA-A2, we reasoned this variant would resist a register shift. Consistent with this reasoning, the M9A substitution nearly ablated TCR recognition (Supplementary Table 3). We next examined a variant in which the p10 methionine was replaced with valine. As valine is a superior HLA-A2 anchor, we reasoned this variant would also resist a register shift. No TCR binding was detected with the M10V substitution, and notably, the M10V substitution significantly strengthened peptide binding to HLA-A2, raising the T_m of the pMHC complex 12 °C (Supplementary Table 3).

A third variant we examined was a C-terminal truncation of MMWDRGLGMM, yielding a nonamer missing the p10 methionine. This peptide we hypothesized would adopt the TCR-bound nonameric configuration in the free pMHC, promoting TCR binding. The truncated peptide was recognized with an affinity close to the native peptide (Supplementary Table 3), but with distinct kinetics, including a faster association rate, consistent with the lack of a register shift (Supplementary Figure 2).

We further probed the mechanism of the MMWDRGLGMM register shift with two additional variants. Although it is fully buried in the MHC binding groove, changing the p7 leucine to alanine weakened TCR binding to non-quantifiable levels (K_D > 500 μM), consistent with our hypothesized role of pLeu7 in distorting the HLA-A2 α2 helix and facilitating the register shift. Replacing the p5 arginine with alanine weakened TCR binding similarly, supporting the hypothesis that TCR-forced movement of Arg5 catalyzes peptide and HLA-A2 conformational reorganization (Supplementary Table 3).

DMF5 accommodation of the two peptide classes

Compared to the MART-1 and SMLGIGIVPV GIG complexes, DMF5 binds the register-shifted MMWDRGLGMM/HLA-A2 complex such that the TCR is shifted approximately 2 Å towards the peptide N-terminus (Figure 6A). The shift in TCR position allows the receptor to form similar hydrogen bonds between Gln30 of CDR1α and the backbones of peptide positions 2 and 4. The peptide-Q30 interactions are the most clearly shared TCR-peptide interactions between the GIG and DRG interfaces.

Although the TCR binding position is slightly shifted, the TCR CDR loops themselves do not change: the RMSD for all atoms of the CDR loops is only 1.0 Å when the TCRs from the SMLGIGIVPV and MMWDRGLGMM complexes are superimposed. This conserved CDR loop geometry is consistent with previous determinations that the backbones of the DMF5 binding loops are comparatively rigid compared to other, more flexible TCRs [26].

Of interest is how the charges present in the MMWDRGLGMM peptide but absent in GIG peptides are accommodated by the DMF5 TCR. In binding MMWDRGLGMM, the side chain of Asp91 of CDR3α rotates away from the peptide to avoid repulsion from the p4 aspartic acid (Figure 6B). The p4Asp hydrogen bonds with Gly93 of CDR3α, mimicking a role played by a water molecule present in the SMLGIGIVPV complex that links CDR3α to the pGly4 backbone. A new buried water molecule links pAsp4 to the TCR, forming a bridged hydrogen with Gly93 of CDR3α. As noted in Figure 4, in the MMWDRGLGMM complex the arginine at p5 has been pushed to the side of the interface. Here, it forms a water-bridged hydrogen bond with the carbonyl of Ala150 of HLA-A2, explaining the return of the α2 helix to a more traditional conformation and offsetting the loss of TCR-peptide hydrogen bonds seen in the GIG complexes but not in the MMWDRGLGMM complex.

The crucial water molecule that bridges the TCR and peptide center in the GIG complexes (Figure 4) cannot fit in the MMWDRGLGMM complex due to the position of the peptide backbone. Instead, the amide nitrogen of pGly6 forms one of the same hydrogen bonds, linking the peptide backbone to Phe100β. The side chain of Asn33β is rotated away from the interface to avoid clashes with pMet10 in its new position (the movement of Asn33β to accommodate the register-shifted decamer may explain why the TCR binds the truncated MMWDRGLGM nonamer with an affinity similar to the decamer (Figure 5D), even though the nonamer is locked in the register-shifted conformation). Overall then, a combination of small TCR side chain adjustments, differential use of water, and HLA-A2 plasticity explain how the very different GIG and register shifted-DRG surfaces are both recognized by the DMF5 TCR.

Although the receptor is slightly N-terminally shifted when bound to MMWDRGLGMM as shown in Figure 6A, there are no major alterations in how the TCR engages the HLA-A2 protein. For example, signature TCR-HLA-A2 interactions involving Tyr51 in CDR2β, Arg65 in the HLA-A2 α1 helix, and a negative charge in CDR1α are unchanged between the MMWDRGLGMM and GIG complexes (Supplementary Figure 4). These conserved TCR interactions with HLA-A2, previously shown to help drive TCR recognition of HLA-A2 and restrict its binding orientation [34], also likely play an important role in facilitating DMF5 cross-reactivity with the DRG and GIG class of peptides as discussed below.

Superimposing the unbound and bound MMWDRGLGMM/HLA-A2 complexes confirms that multiple clashes help drive the peptide register shift. The clashes involve the peptide backbone at pAsp4 and the side chain of pArg5, both of which clash with residues of CDR3β. The most severe clashes involve pArg5, which occupies the same volume as the backbone of Gly101β and Thr102β (Figure 6C).

Discussion

Although T cell specificity is a hallmark of cellular immunity, TCRs themselves are cross-reactive [4, 5]. Recently, we described how TCR cross-reactivity can be accounted for by considering the structural biophysics of TCR interfaces [5]. In cross-reacting, TCRs have appeared to focus on structurally and chemically homologous peptide regions, sometimes facilitated by conformational changes, which allows for formation of similar if not identical

interatomic interactions. The resulting restrictions on ligand diversity bring the pool of compatible ligands for any one TCR down from a theoretical upper limit in the billions to the experimentally observed size in the millions, with many compatible ligands sharing little sequence identity but significant structural and chemical similarity [5]. This scenario is exemplified by DMF5 recognition of different GIG class of peptides.

The identification of the highly distinctive DRG class of peptides as ligands for the DMF5 TCR was therefore unexpected. Although hints of such behavior have been seen in other studies of TCR cross-reactivity [16, 17], the identification of such highly distinctive classes of peptides for one TCR pushes against the TCR cross-reactivity paradigm that has emerged. The finding that DMF5 can cross-react with such disparate classes of peptides is thus a cautionary demonstration that the pools of ligands available to any given TCR can be larger than estimated from considerations based solely on sequence, chemical, or even structural similarity.

Protein conformational adaptability is one mechanism by which one protein can bind different ligands. Conformational adaptability has been shown numerous times to contribute to TCR cross-recognition, with changes observed in the receptor, the peptide, and the MHC protein [20, 21]. Protein adaptability is indeed required for DMF5 cross-recognition between the GIG and DRG classes of peptides. Yet unexpectedly, in recognition of MMWDRGLGMM adaptability occurs in the peptide, which undergoes a dramatic register shift that allows the decameric peptide to move into a new conformation with the C-terminus extending from the end of the binding groove. The register shift is in turn facilitated by conformational adjustments in the presenting HLA-A2 protein. TCR cross-reactivity between different pools of ligands can therefore be facilitated by heretofore unanticipated peptide/MHC conformational changes, to include register shifts at the peptide C-terminus, TCR binding-induced peptide extensions from class I MHC peptide binding grooves, and corresponding adjustments in the MHC.

The mechanism of the register shift and resulting C-terminal extension in the MMWDRGLGMM peptide is attributable to multiple peptide features. The leucine at position 7 is positioned in a way that destabilizes the HLA-A2 α2 helix and the nearby F pocket (Figure 2B). This region of class I MHC proteins is especially pliable, with displacements and even C-terminal extensions observed in other pMHC structures [13, 14, 33, 35–37]. Additionally, the C-terminal anchor of the peptide is methionine, which is larger than the more preferred valine [38]. The use of methionine as an anchor elevates the C-terminal half of the peptide away from the base of the binding groove, further destabilizing the pMHC complex. A similar elevation of the peptide away from the HLA-A2 groove has been seen in other instances where methionine is used as a C-terminal anchor [39]. The MMWDRGLGMM/HLA-A2 complex is thus “primed” for a register-shifting slip upon TCR binding. The slip is triggered by the need for the bulky p5 arginine to move away from the rigid DMF5 TCR as it binds, which in turn requires the peptide backbone to move out of the way to avoid a steric clash. In moving, the arginine helps return the HLA-A2 α2 helix back to its usual conformation, and the presence of a methionine at the penultimate peptide position provides for a suitable, if suboptimal, anchor for the HLA-A2 F pocket. Although described linearly, it is likely that multiple aspects of this mechanism occur simultaneously

during binding, facilitated by a less stable, dynamic pMHC complex. The extent to which this mechanism and the surrounding structural details is applicable to DMF5 recognition of other peptides in the DRG-class is not known. However, the sequence, structural, and physical similarities between the DRG peptides suggest elements of this mechanism will be shared between peptides, even if fine details diverge.

The shift in the MMWDRGLGMM peptide does not bring it into a conformation that mimics the MART-1 or other peptides in the GIG class as seen in instances of "induced-fit molecular mimicry" [32, 40]. How does the DMF5 TCR accommodate these different surfaces? Notably, not through large CDR loop conformational changes or global TCR repositioning as seen in other studies [20, 21, 25, 41–44]. Instead, TCR side chain rotations occur to optimize electrostatics and avoid clashes. Water is used differentially in the two interfaces, reinforcing the importance of solvent in allowing TCRs to fit alongside pMHC complexes [45, 46]. One interaction that is conserved between the MMWDRGLGMM and GIG interfaces involves the germline CDR1α loop and the peptide backbone near the N-terminus. The conservation of this interaction, which is also seen in other structures with *TRAV12-2* TCRs [12, 47, 48], is consistent with suggestions that biases towards certain peptide features are present within the TCR repertoire [47–49]. Other shared interactions between the two types of interfaces are evolutionarily-conserved interactions between the TCR CDR loops and charges on the HLA-A2 α1 helix which help orient the TCR over the pMHC [34].

In summary, our findings demonstrate how a single TCR can recognize distinct classes of peptides presented by a common MHC protein, an observation which most clearly captures the concept of immune polyspecificity [1]. Although details will of course differ, our observations are generalizable to TCRs at large: any one class of peptides recognized by a receptor will incorporate many peptides sharing structural and chemical features in the core region [5]. Multiple peptide classes can be recognized, however. Peptides that typify different classes need not share significant similarities, with the TCR relying on structural adaptability, buried water, and conserved interactions with peptide and MHC to engage them. Adaptability is clearly not limited to conformational changes in the TCR but can also include rearrangements such as binding induced peptide register shifts and subsequent extensions from the peptide binding groove. These general lessons have implications for our understanding of TCR specificity and cross-reactivity and highlight new challenges in efforts to rationalize or modulate TCR molecular recognition, as well as efforts to predict epitope immunogenicity.

Online Methods

Structural modeling and energetic scoring

Structural modeling of GIG and DRG peptide/HLA-A2 complexes was performed using Rosetta with the Talaris2013 score function using the PyRosetta interface [50]. Using the 'relax' protocol, five cycles of backbone minimization and rotamer optimization brought the PDB 4JFO template structure to a local energy minimum. Following minimization, the desired peptide sequence, taken from the list of GIG and DRG peptides, was computationally introduced. This was followed by 50 Monte Carlo-based simulated annealing steps for the peptide backbone. For more thorough structural sampling, we

introduced random phi/psi perturbations to the peptide backbone, followed by refinement via the Rosetta LoopMover_Refine_KIC protocol, generating 1000 independent decoys per peptide. Of these, the lowest energy structures were retained for further analysis. The final models were ranked relative to each other for peptide binding affinity using a previously published score function parameterized for quantifying the strength of protein-protein interactions [51].

Proteins and peptides

Soluble DMF5 and HLA-A2 were produced from bacterially expressed inclusion bodies as previously described [52]. Briefly, inclusion bodies for the TCR α and β chains, the HLA-A2 heavy chain, and β_2m were expressed in *Escherichia coli*. Inclusion bodies were isolated and denatured in 8 M urea. For refolding of the TCR, 1:1 ratios the α and β chains were diluted in 50 mM Tris (pH 8), 2 mM EDTA, 2.5 M urea, 9.6 mM cysteamine, 5.5 mM cystamine, and 0.2 mM PMSF. For refolding of the pMHC complexes, 1:1 ratios of the HLA-A2 heavy chain and β_2m were diluted in 100 mM Tris (pH 8), 2 mM EDTA, 400mM L-arginine, 6.3 mM cysteamine, 3.7 mM cystamine, and 0.2 mM PMSF in the presence of three molar excess peptide. TCR and pMHC complexes were incubated for 24 hours at 4 °C. Afterward, complexes were desalted by dialysis at room temperature, then purified by anion exchange followed by size-exclusion chromatography utilizing Superdex 200 and 75 columns. Refolded protein absorptions at 280 nm were measured spectroscopically and concentrations determined with appropriate extinction coefficients. Peptides were obtained from AAPPTec and Chi Scientific, purified to 90% purity, and stored at 30 mM in 100% DMSO at −80 °C. All experiments with the MART-1 peptide used the anchor-modified MART-1 decamer.

Thermal stability measurements

Peptide binding to HLA-A2 was assessed via thermal stability using differential scanning fluorimetry as described previously [53]. Thermal stability measurements probe the strength of peptide binding due to the thermodynamic linkage between ligand binding and protein unfolding, and when tested with peptide-MHC interactions, T_m values from thermal stability measurements correlate well with experimentally determined affinity measurements [54]. Briefly, 10-20 μM purified pMHC buffered in 10 mM HEPES (pH 7.4), 150 mM NaCl, 3 mM EDTA, with 0.005% surfactant P-20 was incubated with 10× excess SYPRO Orange for a total solution volume of 20 μL. Thermal stability was then measured using a Step One Plus qPCR instrument. The scan rate was at 1 °C/minute and fluorescence intensity was recorded at 607 nm. The temperature range spanned from 25 °C to 95 °C. Data were analyzed by fitting the temperature derivative of fluorescence to a bi-Gaussian response function as described previously [53]. The T_m values in Supplementary Table 2 reflect single measurements with errors reported as standard errors after non-linear curve fitting.

Surface plasmon resonance binding data and analysis

Surface plasmon resonance experiments were performed with Biacore 3000 or T200 instruments using CM5 sensor chips. In all experiments, the DMF5 TCR was immobilized on the sensor chip via standard amine coupling and pMHC complexes were injected as analyte. Experiments were performed in 20 mM HEPES (pH 7.4), 150 mM NaCl, and 0.005% surfactant P-20. Both kinetic and steady-state experiments were performed with

TCRs coupled onto to the sensor chip at 50–2000 response units, with lower values used for kinetic experiments to minimize mass transport and rebinding effects. Injected pMHC spanned concentration ranges of 0.1 – 150 μM and flow rates spanned 5-40 μL/min. Data were collected at 25 °C, except when used to determine kinetics, where the temperature was 10 °C.

For equilibrium binding experiments, we used a previously described global analysis procedure to enhance accuracy and precision when measuring weak to moderate binding affinities [55, 56]. Briefly, for each experiment in Supplementary Tables 2 and 3, the activity of each TCR sensor surface (RU_{max}) was determined via a titration with the highest affinity MART-1/HLA-A2 complex. Two independent sets of injections over this same DMF5 TCR surface were then performed, and both sets of data were globally fit to a 1:1 binding model for a single, shared K_D, with the RU_{max} parameter fixed from the previous determination. Errors for equilibrium measurements were standard errors from the global fitting for K_D, or were propagated from K_D errors for determining errors in ΔG°. Data were processed with BiaEvaluation 4 and fit using MATLAB 2015b. In the case of the M9A, L7A, and R5A variants of the MMWDRGLGMM peptide, very weak binding was indicated and the K_D was estimated to be > 500 μM. In the case of the M10V variant, no binding was detected.

Kinetic experiments were performed at 10 °C due to the fast rates. For kinetic experiments, injections of the series of concentrations indicated in Supplementary Figure 2 were performed over common DMF5 TCR surfaces. Data were processed using BiaEvaluation 4 and dissociation rates for each peptide/HLA-A2 complex from the TCR determined by global fitting of all dissociation curves in a series to a single-exponential decay using MATLAB 2015b. Errors in k_{off} were standard errors from global fitting. Association rates were calculated using the separately determined K_D and k_{off} values. Errors in k_{on} were determined by propagating errors in K_D and k_{off}.

Cell lines, media, and reagents

293GP, PG13, and T2 cell lines were obtained from American Type Culture Collection. 293GP cells were maintained in DMEM medium supplemented with 10% FBS. PG13 cells were maintained in IMEM supplemented with 10% FBS. T2 cells were maintained in RPMI-1640 supplemented with 10% FBS. PBMCs used for transduction were purchased from Key Biologics as apheresis products. T cells were isolated by Ficoll-Hypaque density centrifugation. T cells were maintained in AIM-V medium supplemented with 5% heat-inactivated hAB serum, 300 IU/mL rhIL-2 and 100 ng/mL rhIL-15 at 37 °C with 5% CO_2. T cells were OKT3 activated for 3 days with 50 ng/mL anti-CD3 mAb prior to retroviral transduction.

T cell retroviral transduction

T cells were transduced from retroviral supernatant as previously described [57]. Briefly, the DMF5 TCR α chain and β chain were linked to truncated CD34 by P2A and T2A self-cleaving sequences, respectively, and inserted into the SAMEN retroviral vector. 3×10^6 293GP cells were cotransfected with 20 μg retroviral DNA and 5 μg of plasmid containing vesicular stomatitis virus envelope gene using 50 μL Lipofectamine 2000. Cells were

incubated at 37 °C in 5% CO_2 and media was replaced six hours post-transfection. Viral supernatant was collected 48 hours post-transfection and filtered. Positive PG13 cells were sorted by a FACSAria instrument with anti-CD34-PE mAb. Transfected PG13 cells (8×10^8 / flask) in IMDM/10% FBS were supplemented with 1 mM sodium butyrate for 8-10 hours, after which media was replaced. Viral supernatant was collected the next day and filtered. T cell transduction was performed by spinoculation. Briefly, 24-well culture plates were coated with 0.5 mL/well 30 μg/mL retronectin overnight at 4 °C. Plates were blocked with 0.5 mL/well PBS containing 2% BSA for 30 min at room temperature, then washed with 2 mL/well PBS. 2 mL/well filtered viral supernatant was added to each well and the plate was spun at 2000 g for two hours at 32 °C. The solution was aspirated and 2 million T cells in 1 mL RPMI/10% FBS were added along with 1 mL of filtered viral supernatant. Plates were spun at 2000 g for two hours at 32 °C incubated overnight. Cells were then transferred to tissue culture-treated flasks with fresh RPMI/10% FBS and incubated for three days.

Functional assays

IFNγ release by DMF5 TCR transduced T cells was analyzed as previously described [58]. Briefly, 1×10^5 T2 cells were pulsed with 10 μM peptide and incubated at 37 °C for two hours. The cells were then washed twice to remove excess peptide. T2 cells were then placed into a 96-well plate and cocultured with an equal number of T cells with 10 ng/mL PMA. The plates were incubated for 20 hours at 37 °C. Final concentrations of secreted IFNγ were measured by ELISA. All samples were assayed in triplicate.

X-ray crystallography and structure analysis

Crystals of the DMF5-SMLGIGIVPV/HLA-A2 complex were grown from 13% PEG 3350, 0.25 M $MgCl_2$ buffered with 0.1 M Tris (pH 8.1) at 25 °C. Crystals of the DMF5-MMWDRGLGMM/HLA-A2 complex were grown from 18% PEG 3350, 0.25 M $MgCl_2$ buffered with 0.1 M HEPES (pH 7.9) at 25 °C. Crystals of the free MMWDRGLGMM/HLA-A2 complex were grown from 25% PEG 1000, 0.01% sodium azide buffered with 0.1 M MES (pH 6.5) at 25 °C. Crystallization was performed using hanging drop/vapor diffusion utilizing a Mosquito crystallization robot with humidity control. For cryoprotection, crystals were transferred into 20% glycerol/80% mother liquor for 30 seconds and flash frozen in liquid nitrogen. Diffraction data were collected at the 22ID (SER-CAT) beamline at the Advanced Photon Source, Argonne National Laboratories. Data reduction was performed with HKL2000. The complexes were solved by molecular replacement using PHENIX and PDB entry 3QDG stripped of the peptide (TCR complexes) or peptide and TCR (pMHC complex) as the reference model. Rigid body refinement, followed by multiple steps of restrained refinement were performed with phenix.refine. Atomic positioning was verified with an iterative-build composite OMIT or feature-enhanced maps calculated in PHENIX. Evaluation of models and fitting to maps were performed using Coot. Structures were visualized using PyMOL or Discovery Studio, and the data deposited to the Protein Data Bank with ascension codes as indicated in the Data Availability section. Supplementary Video 1, illustrating the TCR binding-induced register shift in the peptide, was generated in PyMOL using the rigimol module paired with a refinement step to minimize VDW clashes. For generating the video, 200 interpolation

frames were generated, with coordinates of molecule one of the free pMHC used as frame 1 and the pMHC coordinates of the bound structure used as frame 200. Contacts and hydrogen bonds were evaluated using the Contpro and PISA web servers.

Statistics

Crystallographic statistics were determined and are presented according to accepted practices, as indicated in Supplementary Table 3. Binding and functional data were replicated as indicated. Nonlinear least squares fitting was used to evaluate binding and thermal stability data, with goodness-of-fit determined by minimizing the χ^2 statistic followed by inspection of residuals. Linear correlations between variables were assessed using the R^2 statistic as presented. Error propagation was performed using standard techniques using parameter error and partial derivatives with respect to parameter [59].

Data Availability

Crystallographic datasets are available in the PDB repository under ascension codes 6AMT (MMWDRGLGMM/HLA-A2), 6AMU (DMF5-MMWDRGLGMM/HLA-A2), and 6AM5 (DMF5-SMLGIGIVPV/HLA-A2). Other data are available from the corresponding author upon request.

Supplementary Material

Refer to Web version on PubMed Central for supplementary material.

Acknowledgements

Supported by NIH grants GM118166 and AI29543 (B. Baker); CA154778 and CA153789 (M. Nishimura); and AI103867 (K. C. Garcia); and American Cancer Society grant IRG-14-195-01 (L. Hellman). T. Riley and J. Alonso were supported by fellowships from the Indiana CTSI, funded in part by NIH grants TR001107 and TR001108. M. Gee was supported by a Stanford Graduate Research Fellowship and NIH grant CA216926. J. Mendoza was supported by NIH grant CA175127. K. C. Garcia is supported by the Howard Hughes Medical Institute and the Parker Institute for Cancer Immunotherapy.

References

1. Wucherpfennig KW et al. Polyspecificity of T cell and B cell receptor recognition. Seminars in Immunology 19, 216–224 (2007). [PubMed: 17398114]
2. Mason D A very high level of crossreactivity is an essential feature of the T-cell receptor. Immunology Today 19, 395–404 (1998). [PubMed: 9745202]
3. Sewell AK Why must T cells be cross-reactive? Nat Rev Immunol 12, 669–677 (2012). [PubMed: 22918468]
4. Wooldridge L et al. A Single Autoimmune T Cell Receptor Recognizes More Than a Million Different Peptides. Journal of Biological Chemistry 287, 1168–1177 (2012). [PubMed: 22102287]
5. Singh NK et al. Emerging Concepts in TCR Specificity: Rationalizing and (Maybe) Predicting Outcomes. The Journal of Immunology 199, 2203–2213 (2017). [PubMed: 28923982]
6. Maynard J et al. Structure of an autoimmune T cell receptor complexed with class II peptide-MHC: insights into MHC bias and antigen specificity. Immunity 22, 81–92 (2005). [PubMed: 15664161]
7. Linette GP et al. Cardiovascular toxicity and titin cross-reactivity of affinity-enhanced T cells in myeloma and melanoma. Blood 122, 863–871 (2013). [PubMed: 23770775]

8. Adams JJ et al. Structural interplay between germline interactions and adaptive recognition determines the bandwidth of TCR-peptide-MHC cross-reactivity. Nat Immunol 17, 87–94 (2016). [PubMed: 26523866]
9. Birnbaum Michael E. et al. Deconstructing the Peptide-MHC Specificity of T Cell Recognition. Cell 157, 1073–1087 (2014). [PubMed: 24855945]
10. Cole DK et al. Hotspot autoimmune T cell receptor binding underlies pathogen and insulin peptide cross-reactivity. The Journal of Clinical Investigation 126, 2191–2204 (2016). [PubMed: 27183389]
11. Hausmann S et al. Peptide recognition by two HLA-A2/Tax11-19-specific T cell clones in relationship to their MHC/peptide/TCR crystal structures. J Immunol 162, 5389–5397 (1999). [PubMed: 10228016]
12. Garboczi DN et al. Structure of the complex between human T-cell receptor, viral peptide and HLA-A2. Nature 384, 134–141 (1996). [PubMed: 8906788]
13. Borbulevych OY, Piepenbrink KH & Baker BM Conformational Melding Permits a Conserved Binding Geometry in TCR Recognition of Foreign and Self Molecular Mimics. J Immunol 186, 2950–2958 (2011). [PubMed: 21282516]
14. Borbulevych OY et al. T cell receptor cross-reactivity directed by antigen-dependent tuning of peptide-MHC molecular flexibility. Immunity 31, 885–896 (2009). [PubMed: 20064447]
15. Frankild S, de Boer RJ, Lund O, Nielsen M & Kesmir C Amino Acid Similarity Accounts for T Cell Cross-Reactivity and for “Holes” in the T Cell Repertoire. PLOS ONE 3, e1831 (2008). [PubMed: 18350167]
16. Rubio-Godoy V et al. Positional Scanning-Synthetic Peptide Library-Based Analysis of Self- and Pathogen-Derived Peptide Cross-Reactivity with Tumor-Reactive Melan-A-Specific CTL. The Journal of Immunology 169, 5696–5707 (2002). [PubMed: 12421949]
17. Dutoit V et al. Degeneracy of Antigen Recognition as the Molecular Basis for the High Frequency of Naive A2/Melan-A Peptide Multimer+ CD8+ T Cells in Humans. J Exp Med 196, 207–216 (2002). [PubMed: 12119345]
18. Brehm MA et al. T cell immunodominance and maintenance of memory regulated by unexpectedly cross-reactive pathogens. Nat. Immunol 3, 627 (2002). [PubMed: 12055626]
19. Clute SC et al. Broad Cross-Reactive TCR Repertoires Recognizing Dissimilar Epstein-Barr and Influenza A Virus Epitopes. The Journal of Immunology 185, 6753–6764 (2010). [PubMed: 21048112]
20. Miles JJ, McCluskey J, Rossjohn J & Gras S Understanding the complexity and malleability of T-cell recognition. Immunol Cell Biol 93, 433–441 (2015). [PubMed: 25582337]
21. Armstrong KM, Piepenbrink KH & Baker BM Conformational changes and flexibility in T-cell receptor recognition of peptide-MHC complexes. Biochem J 415, 183–196 (2008). [PubMed: 18800968]
22. Johnson LA et al. Gene Transfer of Tumor-Reactive TCR Confers Both High Avidity and Tumor Reactivity to Nonreactive Peripheral Blood Mononuclear Cells and Tumor-Infiltrating Lymphocytes. J Immunol 177, 6548–6559 (2006). [PubMed: 17056587]
23. Johnson LA et al. Gene therapy with human and mouse T-cell receptors mediates cancer regression and targets normal tissues expressing cognate antigen. Blood 114, 535–546 (2009). [PubMed: 19451549]
24. Chodon T et al. Adoptive Transfer of MART-1 T-Cell Receptor Transgenic Lymphocytes and Dendritic Cell Vaccination in Patients with Metastatic Melanoma. Clinical Cancer Research 20, 2457–2465 (2014). [PubMed: 24634374]
25. Borbulevych OY, Santhanagopolan SM, Hossain M & Baker BM TCRs Used in Cancer Gene Therapy Cross-React with MART-1/Melan-A Tumor Antigens via Distinct Mechanisms. J Immunol 187, 2453–2463 (2011). [PubMed: 21795600]
26. Ayres CM, Scott DR, Corcelli SA & Baker BM Differential utilization of binding loop flexibility in T cell receptor ligand selection and cross-reactivity. Scientific Reports 6, 25070 (2016). [PubMed: 27118724]
27. Gee MH et al. Antigen Identification for Orphan T Cell Receptors Expressed on Tumor-Infiltrating Lymphocytes. Cell 172, 549–563.e516 (2018). [PubMed: 29275860]

28. Riley TP et al. A generalized framework for computational design and mutational scanning of T-cell receptor binding interfaces. Protein Engineering Design and Selection 29, 595–606 (2016).
29. Riley TP, Singh NK, Pierce BG, Weng Z & Baker BM in Computational Design of Ligand Binding Proteins. (ed. Stoddard LB) 319–340 (Springer New York, New York, NY; 2016).
30. Sliz P et al. Crystal Structures of Two Closely Related but Antigenically Distinct HLA-A2/Melanocyte-Melanoma Tumor-Antigen Peptide Complexes. J Immunol 167, 3276–3284 (2001). [PubMed: 11544315]
31. Borbulevych OY et al. Structures of MART-1(26/27-35) Peptide/HLA-A2 Complexes Reveal a Remarkable Disconnect between Antigen Structural Homology and T Cell Recognition. J Mol Biol 372, 1123–1136 (2007). [PubMed: 17719062]
32. Macdonald WA et al. T Cell Allorecognition via Molecular Mimicry. Immunity 31, 897–908 (2009). [PubMed: 20064448]
33. McMurtrey C et al. Toxoplasma gondii peptide ligands open the gate of the HLA class I binding groove. eLife 5, e12556 (2016). [PubMed: 26824387]
34. Blevins SJ et al. How structural adaptability exists alongside HLA-A2 bias in the human αβ TCR repertoire. Proceedings of the National Academy of Sciences 113, E1276–E1285 (2016).
35. Smith KJ et al. An Altered Position of the [alpha]2 Helix of MHC Class I Is Revealed by the Crystal Structure of HLA-B*3501. Immunity 4, 203–213 (1996). [PubMed: 8624811]
36. Motozono C et al. Distortion of the Major Histocompatibility Complex Class I Binding Groove to Accommodate an Insulin-derived 10-Mer Peptide. The Journal of Biological Chemistry 290, 18924–18933 (2015). [PubMed: 26085090]
37. Collins EJ, Garboczi DN & Wiley DC Three-dimensional structure of a peptide extending from one end of a class I MHC binding site. Nature 371, 626–629 (1994). [PubMed: 7935798]
38. Sidney J, Peters B, Frahm N, Brander C & Sette A HLA class I supertypes: a revised and updated classification. BMC Immunology 9, 1 (2008). [PubMed: 18211710]
39. Mohammed F et al. Phosphorylation-dependent interaction between antigenic peptides and MHC class I: a molecular basis for the presentation of transformed self. Nat. Immunol 9, 1236 (2008). [PubMed: 18836451]
40. Pellicci DG et al. Recognition of β-linked self glycolipids mediated by natural killer T cell antigen receptors. Nat. Immunol 12, 827 (2011). [PubMed: 21804559]
41. Jones LL, Colf LA, Stone JD, Garcia KC & Kranz DM Distinct CDR3 Conformations in TCRs Determine the Level of Cross-Reactivity for Diverse Antigens, but Not the Docking Orientation. J Immunol 181, 6255–6264 (2008). [PubMed: 18941216]
42. Colf LA et al. How a Single T Cell Receptor Recognizes Both Self and Foreign MHC. Cell 129, 135–146 (2007). [PubMed: 17418792]
43. Rossjohn J et al. T Cell Antigen Receptor Recognition of Antigen-Presenting Molecules. Annual Review of Immunology 33, 169–200 (2015).
44. Reiser JB et al. A T cell receptor CDR3beta loop undergoes conformational changes of unprecedented magnitude upon binding to a peptide/MHC class I complex. Immunity 16, 345–354 (2002). [PubMed: 11911820]
45. Stewart-Jones GB, McMichael AJ, Bell JI, Stuart DI & Jones EY A structural basis for immunodominant human T cell receptor recognition. Nat Immunol 4, 657–663 (2003). [PubMed: 12796775]
46. Rudolph MG, Stanfield RL & Wilson IA How TCRs Bind MHCs, Peptides, and Coreceptors. Annu Rev Immunol 24, 419–466 (2006). [PubMed: 16551255]
47. Bovay A et al. T cell receptor alpha variable 12-2 bias in the immunodominant response to Yellow fever virus. European Journal of Immunology 48, 258–272 (2018). [PubMed: 28975614]
48. Cole DK et al. Germline-governed recognition of a cancer epitope by an immunodominant human T-cell receptor. Journal of Biological Chemistry 284, 27281–27289 (2009). [PubMed: 19605354]
49. Van Braeckel-Budimir N et al. A T Cell Receptor Locus Harbors a Malaria-Specific Immune Response Gene. Immunity 47, 835–847.e834 (2017). [PubMed: 29150238]

Online Methods References

50. Das R & Baker D Macromolecular modeling with rosetta. Annu Rev Biochem 77, 363–382 (2008). [PubMed: 18410248]
51. Kortemme T & Baker D A simple physical model for binding energy hot spots in protein-protein complexes. Proceedings of the National Academy of Sciences of the United States of America 99, 14116–14121 (2002). [PubMed: 12381794]
52. Davis-Harrison RL, Armstrong KM & Baker BM Two Different T Cell Receptors use Different Thermodynamic Strategies to Recognize the Same Peptide/MHC Ligand. Journal of Molecular Biology 346, 533–550 (2005). [PubMed: 15670602]
53. Hellman LM et al. Differential scanning fluorimetry based assessments of the thermal and kinetic stability of peptide-MHC complexes. J Immunol Methods 432, 95–101 (2016). [PubMed: 26906089]
54. Morgan CS, Holton JM, Olafson BD, Bjorkman PJ & Mayo SL Circular dichroism determination of class I MHC-peptide equilibrium dissociation constants. Protein Sci 6, 1771–1773 (1997). [PubMed: 9260291]
55. Blevins SJ & Baker BM Using Global Analysis to Extend the Accuracy and Precision of Binding Measurements with T cell Receptors and Their Peptide/MHC Ligands. Frontiers in Molecular Biosciences 4, 1–9 (2017). [PubMed: 28174697]
56. Piepenbrink KH, Gloor BE, Armstrong KM & Baker BM Methods for Quantifying T Cell Receptor Binding Affinities and Thermodynamics. Methods Enzymol 466, 359–381 (2009). [PubMed: 21609868]
57. Spear TT et al. Hepatitis C virus-cross-reactive TCR gene-modified T cells: a model for immunotherapy against diseases with genomic instability. Journal of Leukocyte Biology 100, 545–557 (2016). [PubMed: 26921345]
58. Cole DJ et al. Characterization of the functional specificity of a cloned T-cell receptor heterodimer recognizing the MART-1 melanoma antigen. Cancer Res 55, 748–752 (1995). [PubMed: 7531614]
59. Bevington PR & Robinson DK Data reduction and error analysis for the physical sciences, Edn. 2nd (McGraw-Hill, New York; 1992).

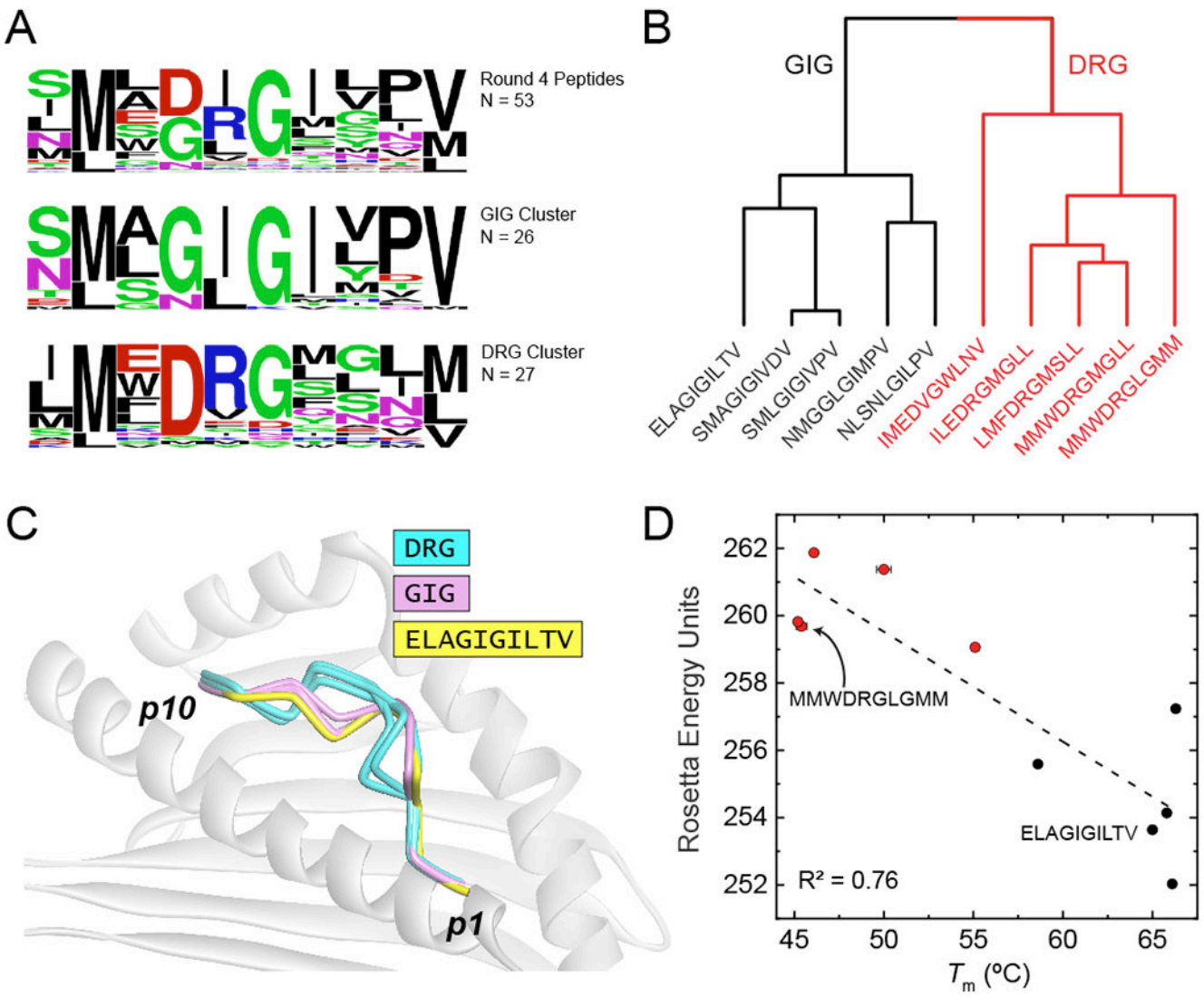

Figure 1. Two distinctive classes of peptides recognized by the DMF5 TCR.

(A) Sequence logos of peptides in the GIG and DRG classes of peptides identified through specificity profiling by yeast display. **(B)** Dendrogram showing the relationships between the GIG (black) and DRG (red) peptide classes. **(C)** GIG and DRG peptides are predicted to adopt different and conformations when bound to HLA-A2, with the conformations of the GIG peptides closely resembling the MART-1 decamer. **(D)** Consistent with the structural modeling, the DRG peptides bind weaker to HLA-A2 as demonstrated by differential scanning fluorimetry (see also Supplementary Table 2). The DSF-determined T_m values correlate with well with structure-based energy scores, supporting the conclusion that the differences in peptide binding are attributable to pMHC structural differences between the two peptide classes. Error bars for the T_m measurements reflect DSF fitting error. R^2 is the coefficient of determination as determined by linear least squares analysis.

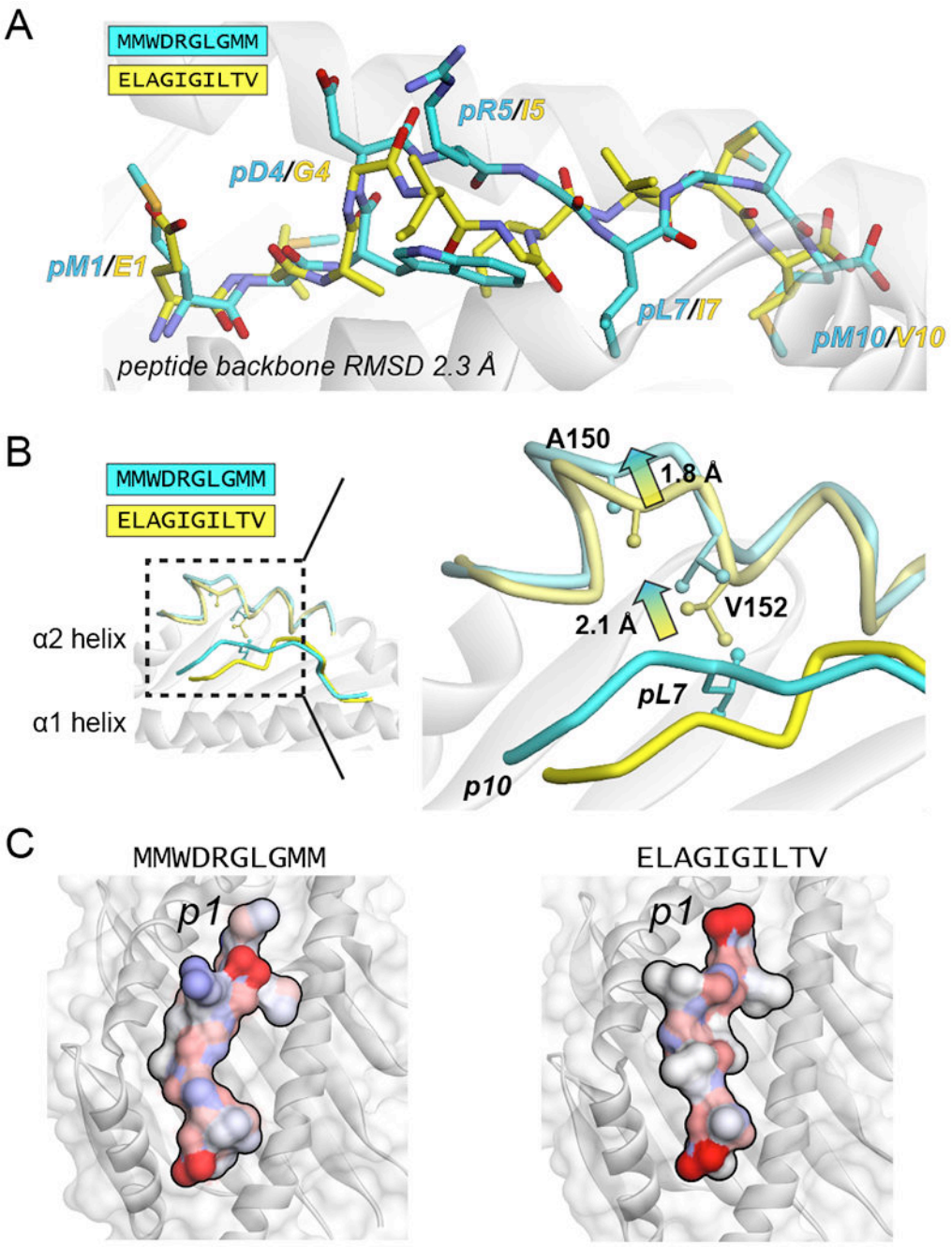

Figure 2. The DRG peptide MMWDRGLGMM adopts a conformation distinct from MART-1 when bound to HLA-A2 and perturbs the structure of the HLA-A2 α2 helix.

(A) Comparison of the crystallographic structures of the MMWDRGLGMM and MART-1 peptides bound to HLA-A2. Compared to MART-1, the MMWDRGLGMM peptide is more bulged and lifted away from the base of the binding groove. The MMWDRGLGMM and MART-1 peptide backbones differ with an RMSD of 2.3 Å when the HLA-A2 peptide binding domains are superimposed. **(B)** The MMWDRGLGMM peptide perturbs the short arm of the HLA-A2 α2 helix. Compared to the structure with MART-1, the position of pL7

in MMWDRGLGMM forces a shift of Val152, which in turn forces the helix away from the peptide, indicated by the 1.8 Å displacement of Ala150. **(C)** The MMWDRGLGMM and MART-1 peptide/HLA-A2 complexes present different surfaces for TCR recognition. Peptide surfaces are colored by partial atomic charge.

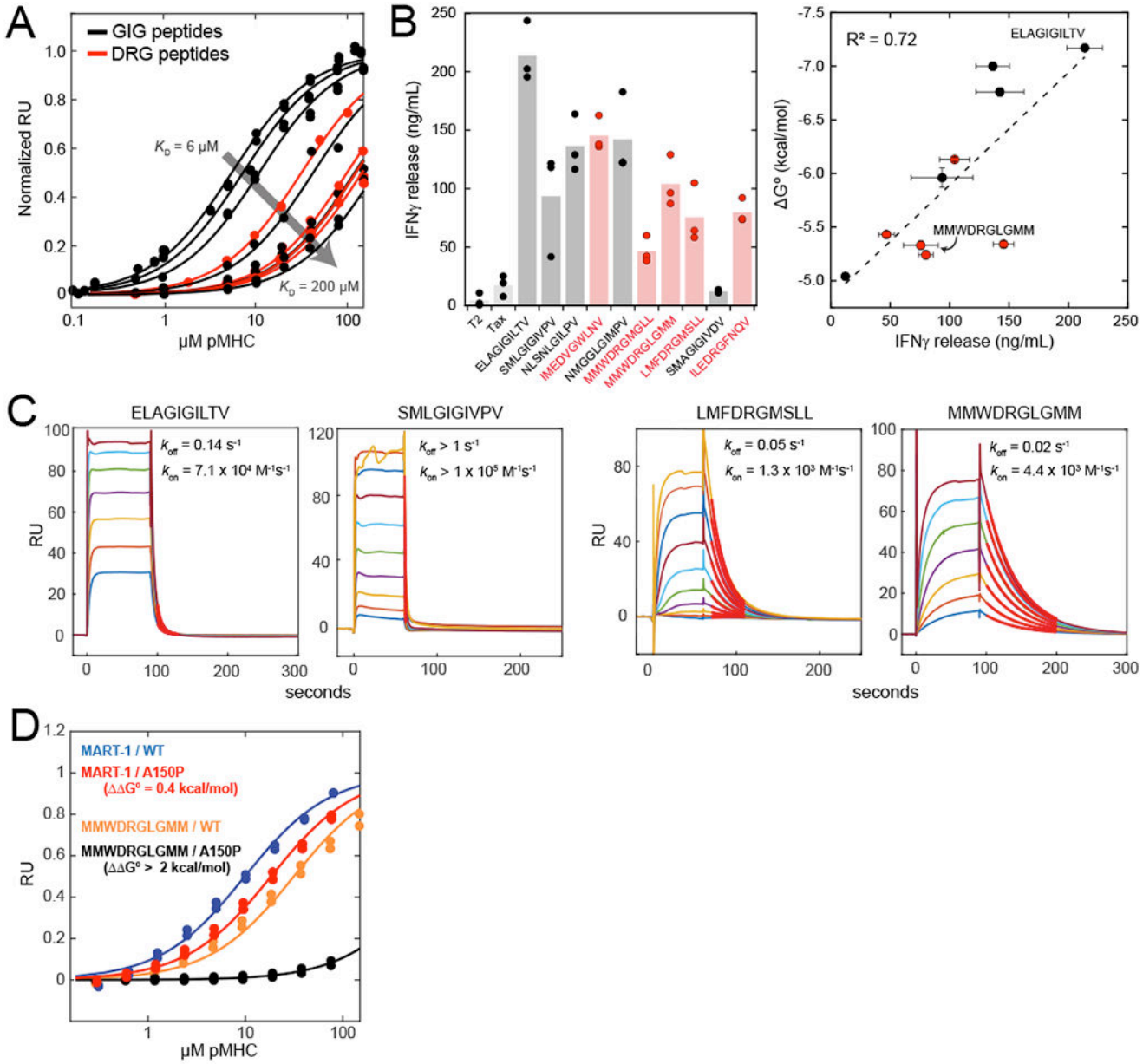

Figure 3. The DMF5 TCR does not show a preference for DRG vs. GIG peptides but the classes are recognized via distinct mechanisms.

(A) SPR binding data for DMF5 recognition of the GIG (black) or DRG (red) peptides. K_D values range from 6 μM for the MART-1 GIG peptide to 200 μM for the SMAGIGIVDV GIG peptide (see also Supplementary Table 2). Unlike the pMHC T_m values, the K_D values do not segregate by peptide class. Each curve indicates a global analysis of two independent replicates as described in the Methods. **(B)** Functional recognition by DMF5-expressing T cells also does not segregate by class and correlates well with TCR binding affinity. The left panel shows IFNγ release for recognition of each peptide, with TCR-transduced PBMCs co-cultured with peptide-pulsed T2 cells. Data for DRG peptides is red. T2 indicates presenting cells without peptide; Tax is a negative control peptide (LLFGYPVYV). Dots show the

values from three independent experiments; bars indicate averages. The right panel shows a plot of ΔG° vs. the mean of the cytokine release experiments. Error bars for IFNγ are SEM from the three experiments shown in the left panel; error bars for ΔG° are propagated K_D errors. R^2 is the coefficient of determination as determined by linear least squares analysis. **(C)** Although DMF5 does not distinguish between recognition of DRG and GIG peptides in binding or function, the peptide classes are recognized with different kinetics. As shown for MART-1 and SMLGIGIVPV in the left panels, GIG peptides are recognized with fast on-rates and fast off-rates. DRG peptides are recognized with slower on and slower off rates, as shown for LMFDRGMSLL and MMWDRGLGMM in the right panels. Thick red lines indicate fits to dissociation phases. Rates are determined from global analysis of the number of separate injections shown in each panel (see Supplementary Figure 2 for full datasets). **(D)** The differential impact of the HLA-A2 A150P mutation confirms HLA-A2 α2 helix shift is important for DMF5 recognition of MMWDRGLGMM but not MART-1. As shown by SPR, the A150P mutation has a minor impact on DMF5 binding to MART-1 (ΔΔG° of 0.4 kcal/mol), but a substantial impact on binding to MMWDRGLGMM (ΔΔG° > 2 kcal/mol). Each curve indicates a global analysis of two independent replicates as described in the Methods.

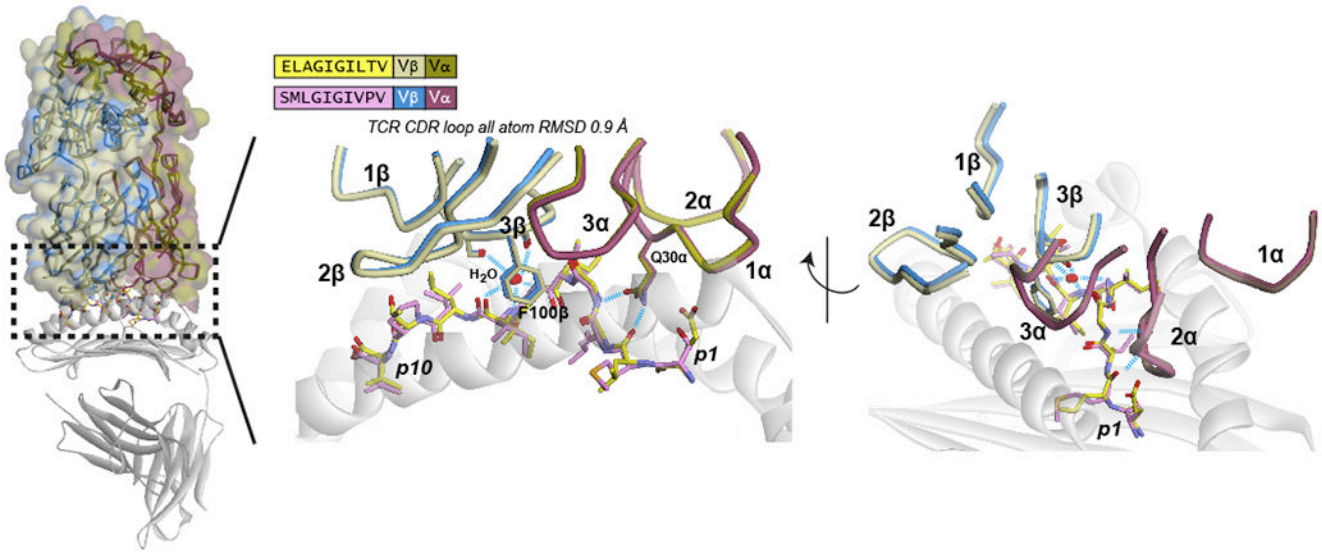

Figure 4. DMF5 recognizes the GIG peptides with common structural solutions.

The TCR-pMHC structure of DMF5 bound to the SMLGIGIVPV peptide is almost identical to the structure of DMF5 bound to MART-1. When the HLA-A2 peptide binding domains are superimposed, all atoms of the CDR loops in the MART-1 and SMLGIGIVPV complexes differ with a RMSD of only 0.9 Å. The SMLGIGIVPV peptide forms many of the same interactions with DMF5 as it does MART-1, including hydrogen bonds from peptide positions 2 and 3 to Gln30 in CDR1α, and both complexes incorporate the same key water molecule that bridges the peptide center and the TCR. Blue dashed lines in the panels indicate hydrogen bonds.

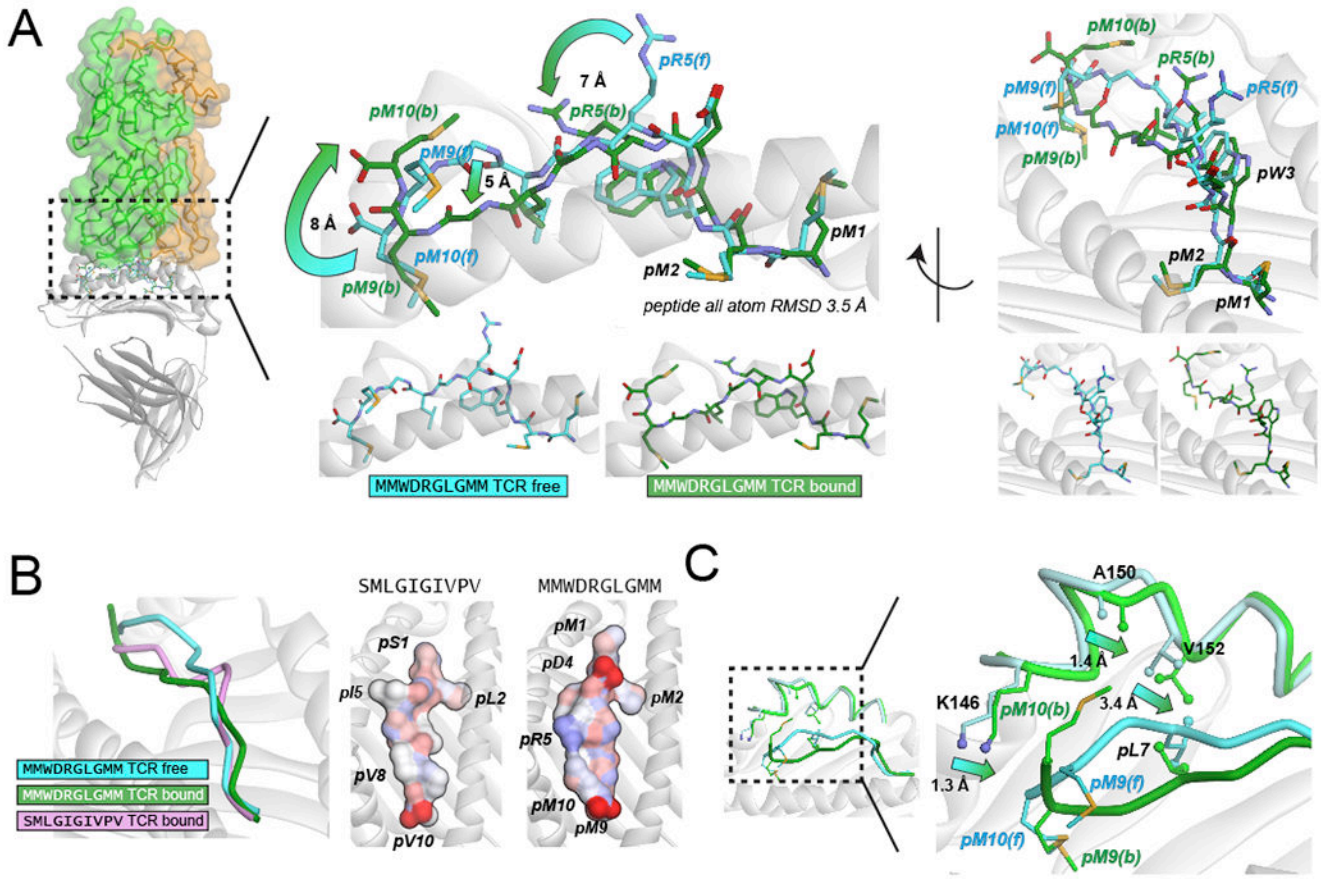

Figure 5. DMF5 recognizes the MMWDRGLGMM DRG peptide very differently, inducing a peptide register shift and C-terminal extension while returning the HLA-A2 α2 helix to its usual conformation.

(A) Illustration of the register shift and C-terminal extension in the MMWDRGLGMM peptide induced upon TCR binding. The side chain of pArg5 moves by 7 Å, the backbone at pGly8 is pressed 5 Å into the base of the binding groove, and the side chain of pMet10 is displaced by 8 Å upon shifting out of the HLA-A2 F pocket. **(B)** The changes in the MMWDRGLGMM peptide seen upon TCR binding bring its conformation closer to but not coincident with the conformation of the GIG peptides, and the TCR-exposed surfaces remain highly distinct. Peptide surfaces are colored by partial atomic charge. **(C)** The HLA-A2 α2 helix returns to a more traditional geometry in the register-shifted MMWDRGLGMM complex, with Lys146, Ala150, and Val152 all moving back towards the center of the binding groove.

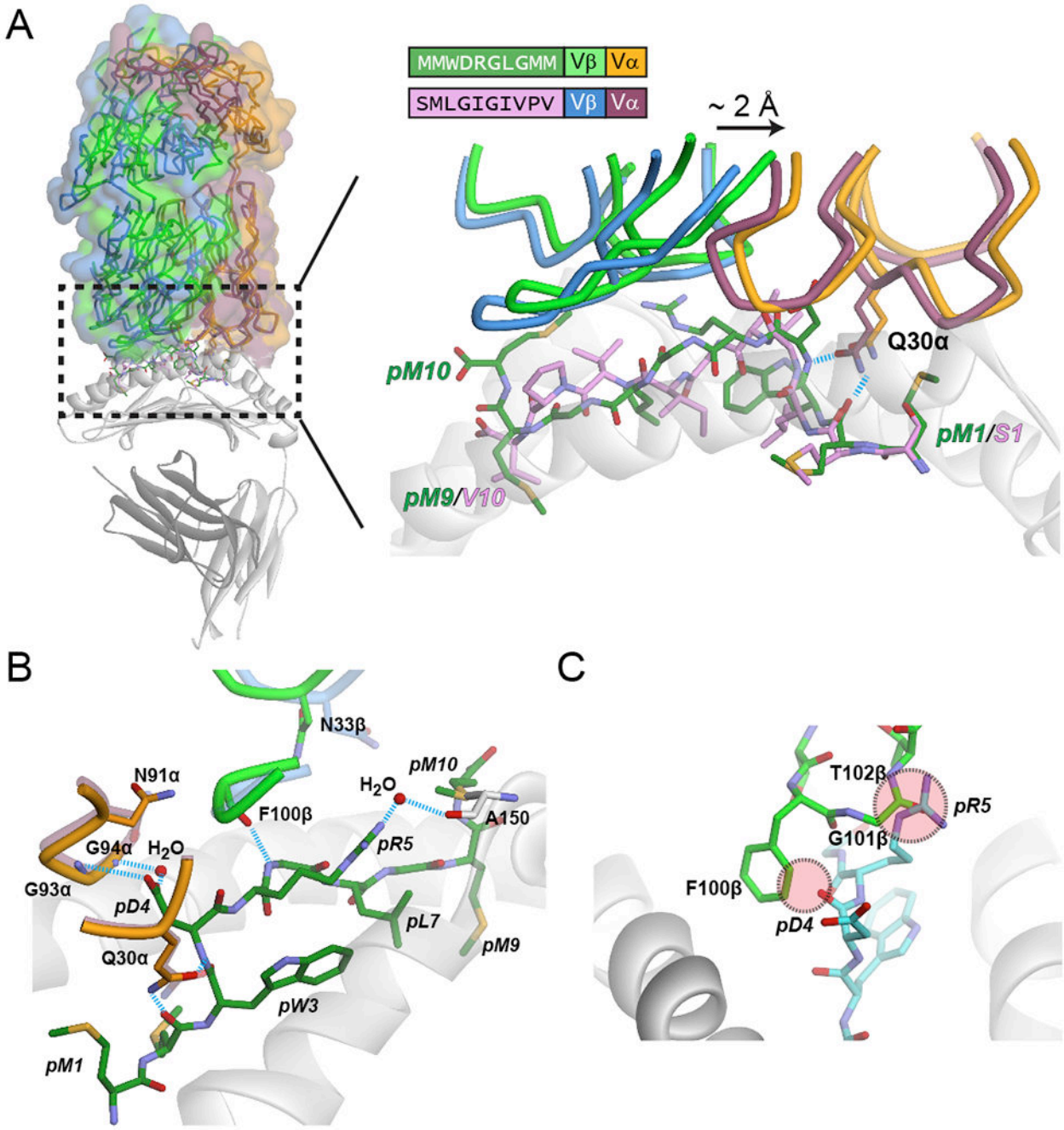

Figure 6. The GIG and register-shifted DRG surfaces are recognized by DMF5 through small TCR side chain rearrangements and differential use of interfacial water.

(A) In the MMWDRGLGMM complex, the DMF5 TCR is positioned 2 Å closer to the peptide N-terminus, but compared to the GIG complexes there are no CDR loop rearrangements. Gln30 of CDR1α forms similar hydrogen bonds with the peptide N-terminal half (blue dashed lines) in the MMWDRGLGMM interface as it does in the GIG interfaces. **(B)** In the MMWDRGLGMM interface, side chain re-arrangements in Asn91α and Asn33β occur to optimize electrostatic and steric complementarity, and new water

molecules are incorporated to meet hydrogen bonding needs. **(C)** Steric clashes between Gly101/Thr102 of CDR3β and pArg5, and Phe100 of CDR3α and pAsp4 drive the conformational change in the MMWDRGLGMM peptide upon TCR binding, as shown in this superimposition of the unbound MMWDRGLGMM peptide into the DMF5-MMWDRGLGMM/HLA-A2 complex.